

SUPPLEMENTARY INFORMATION

Defect dynamics in two-dimensional black phosphorus under argon ion irradiation

Saransh Gupta¹, Prakash Periasamy² and Badri Narayanan¹

¹Department of Mechanical Engineering, University of Louisville, Louisville KY 40223, USA

²Lam Research Inc., Fremont, CA 94538, USA

1. Displacement Threshold Energy

We assess the suitability of ReaxFF for simulating response of phosphorene to ion bombardment by evaluating its accuracy in predicting displacement threshold energy (T_d) for P atoms in ML-phosphorene. Displacement threshold energy T_d is defined as the minimum kinetic energy that must be imparted to a P atom in ML-phosphorene to permanently displace it from its lattice site and form either a self-interstitial (e.g., Frenkel pair) or sputter out yielding a vacancy. To determine T_d , we employ an orthorhombic computational supercell of ML-phosphorene with dimensions $\sim 5.62 \text{ nm} \times 5.92 \text{ nm} \times 5 \text{ nm}$ containing 884 atoms. Periodic boundary conditions are applied in the plane of the sheet, while fixed boundary conditions are used in the direction normal to the sheet. Next, we impart a kinetic energy K to a selected P atom called the primary knock-on (PKA) atom, and monitor the structural evolution of ML-phosphorene over a CMD run of 1.5 ps within the microcanonical (NVE) ensemble following previous works on graphene,¹ h-BN,² and MoS₂.³ We observed that atoms displace negligibly after ~ 1 ps in a single cascade initiated by the PKA. Also, the duration of the CMD runs (i.e., 1.5 ps) is sufficiently long for a PKA to restore to its original position, similar to previous works in 2D materials. We employed several values of K in the range 1 eV to 10 eV, with a resolution of 0.5 eV; and each of the four crystallographically distinct P atoms are treated individually as PKA. For each combination of PKA and selected kinetic energy K , we performed CMD simulations with the initial PKA velocity vectors directed along 20 different directions chosen arbitrarily. The magnitude of the velocity is given by the kinetic energy K . Note, it is assumed that the energy is transferred to the PKA through a binary collision with an incident energetic ion.

The temporal evolution of ML-phosphorene with a representative PKA (shown in red) at different kinetic energies K is depicted in Figure S1. For all values of $K \leq 6$ eV, the PKA initially displaces from its lattice site (Figure S1 (a,b)), but reverts back to its original position within 1.5 ps (Figure S1(c)). At $K = 6.5$ eV, the PKA displaces to form a stable vacancy-interstitial pair

(Frenkel pair) as shown in Figure S1(d-f), indicating that T_d for phosphorene is ~ 6.5 eV. This value of T_d predicted by ReaxFF is in excellent agreement with previous first-principles calculations (that report T_d of 6 eV).⁴ Furthermore, we found that upon subsequent annealing at 700 K, the Frenkel pair shown in Figure S1(f) re-organizes to form a 5|6|7 Stone-Wales defect (Figure S2). Previous first-principles simulations work has reported the formation of a similar SW configuration upon imparting a kinetic energy close to the displacement threshold.⁴

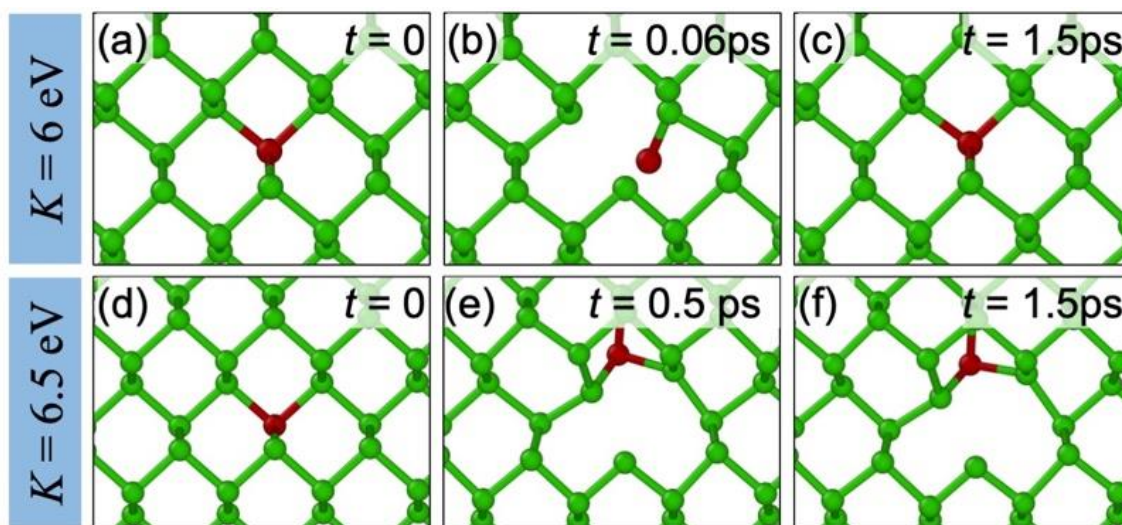


Figure S1. Calculation of displacement threshold for P atom in ML-phosphorene using ReaxFF-CMD simulations. In each simulation, a prescribed kinetic energy (K) is imparted to a given P atom (shown in red; also called primary knock-on atom), and the temporal evolution of the sheet is monitored over a short CMD run. (a-c) Atomic snapshots at three selected timesteps chosen from CMD run at $K = 6$ eV. At all values of $K \leq 6$ eV, the primary knock-on atom displaces initially but returns back to its ideal lattice site within 1.5 ps. (d-f) Atomic snapshots at three selected timesteps chosen from CMD run at $K = 6.5$ eV. At this kinetic energy, the primary knock-on atom gets permanently displaced forming a Frenkel pair shown in panel (f).

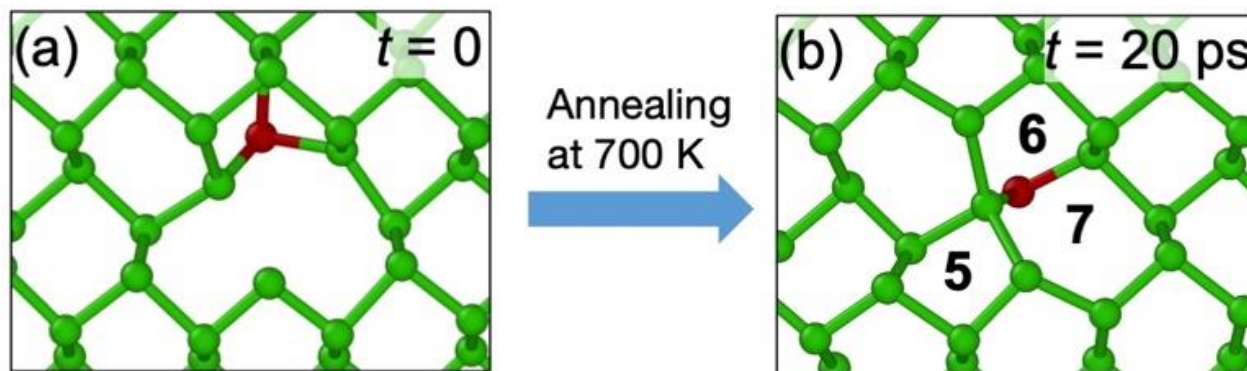


Figure S2. Evolution of a Frenkel defect in Figure S1(f) during subsequent annealing at 700 K

2. Sputtering yield at different kinetic energy of bombarding Ar ion in the single impact limit

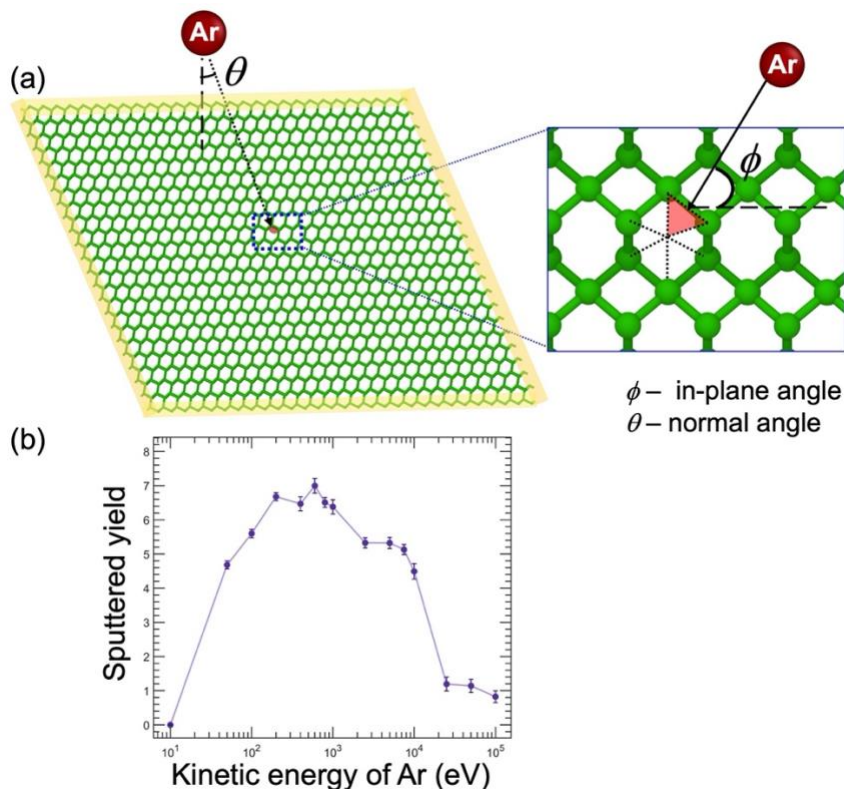


Figure S3 Calculation of sputtering yield in a monolayer of phosphorene due to impact from a single incident Ar ion at various kinetic energies. (a) Argon ion is imparted a prescribed kinetic energy (in the range 0 -100 keV) along a direction defined by normal angle θ and in-plane angle ϕ . Inset of panel (a) shows a selected region of the computational supercell of pristine ML-phosphorene (9.58 nm \times 10 nm \times 5 nm) illustrating the irreducible region (shown in red) within which 100 impact points are randomly chosen. At each chosen kinetic energy value for Ar, we performed 2,000 CMD simulations (100 impact points \times 4 normal angles $\theta \times$ 5 in-plane angles ϕ). (b) Number of phosphorus atoms sputtered from monolayer phosphorene due to impact by a single Ar ion at various ion kinetic energies, as obtained from CMD simulations. The value at each Ar kinetic energy is averaged over 2000 CMD runs; error bars are also provided to show the standard deviation.

To investigate the sputtering yield of ML-phosphorene due to a single Ar-ion impact, we performed CMD simulations with a computational supercell (9.58 nm \times 10 nm \times 5 nm) consisting of 2552 atoms. Periodic boundary conditions are applied in the plane of the sheet, while fixed boundary conditions are used in the direction normal to the sheet. Following previous works on other 2D materials,¹⁻³ we employed CMD simulations within microcanonical ensemble to follow collision cascades initiated by incident Ar ions at various kinetic energies (Figure S3). We chose

15 energies from a wide spectrum of 0 eV to 100 keV. For each energy, a total of 100 random impact points were selected within the minimum reducible area of the phosphorene lattice (Figure S2(a)). Similarly, at each Ar energy, the velocity vector of the incident Ar atom is directed at 20 different directions given by: five random in-plane angles $\phi \in [0^\circ, 360^\circ]$ at each of the four chosen normal angles $\theta = 20^\circ, 40^\circ, 60^\circ, 80^\circ$; this amounts to 2,000 CMD runs for each Ar energy (Figure S3(a)). In all, we employed 30,000 short CMD runs (each 1 ps long). The number of sputtered atoms are evaluated after a short CMD run of 1 ps, based on our observation that atoms displace negligibly after 1 ps for all Ar energies chosen in this study. Since the energy transfer from incident Ar to P atom occurs within the first 0.1 ps, we employed small timestep of 0.025 fs for the first 0.2 ps and 0.5 ps for the remaining 0.8 ps. The P-atoms at the edge of the supercell were held fixed to serve as a heat sink following previous works on graphene^{2,5}.

We found that the dependence of the number of sputtered atoms as a function of Ar-ion energy is qualitatively similar to that in other 2D materials (e.g., graphene,¹ hBN,² and MoS₂³), with maximum sputtering yield of ~ 7 P atoms at an intermediate Ar energy ~ 600 eV (Figure S3(b)). This provides further validation of the approach used in this work to describe atomic interactions. The Ar sputtering yields for phosphorene (maximum of ~ 7) are much higher than in graphene (with a maximum yield ~ 1.2 at Ar energy ~ 300 eV);¹ such high sputtering yields can be attributed to the substantially weaker binding in phosphorene (cohesive energy: -3.48 eV/atom)⁴ than graphene (cohesive energy: -7.76 eV/atom)⁶.

3. Benchmarking the interatomic potentials for Ar-Ar and Ar-P interactions with density functional theory calculations

3.1 Details of density functional theory calculations

We perform density functional theory (DFT) calculations to calculate the binding energy between Ar and P (and Ar and Ar) atoms at various separation distances ($0.5 \text{ \AA} - 4.0 \text{ \AA}$). All DFT calculations are performed using plane-wave formalism within generalized gradient approximation (GGA) as implemented in the VASP package.^{7, 8} To describe the exchange correlation, we employ the Perdew-Burke-Ernzerhof (PBE) functional with the PAW pseudopotentials (Ar: $3s^2 3p^6$, P: $3s^2 3p^3$) supplied by VASP.⁹ The plane wave energy cut off is set at 500 eV, while the Brillouin zone is sampled at Γ point only. At each Ar-P, and Ar-Ar separation, the electronic degrees of freedom are optimized until the energy difference between two successive

self-consistent iterations is less than 10^{-5} eV. Dispersive interactions were accounted using Grimme's D3 correction term.¹⁰

3.2 Ziegler-Biersack-Littmark potential for describing repulsive interaction between Argon and Phosphorus atoms

To describe the repulsive interactions between energetic Ar ions and P atoms in phosphorene, we employ the Ziegler-Biersack-Littmark (ZBL) model, which is developed specifically for high-energy collisions.¹¹ In the framework of ZBL, the potential energy E_{ij}^{ZBL} for a pair of atoms i and j held at a distance r_{ij} apart is expressed as:^{11,12}

$$E_{ij}^{ZBL} = \frac{1}{4\pi\epsilon_0} \frac{Z_i Z_j e^2}{r_{ij}} \phi(r_{ij}/a) + S(r_{ij}),$$

where ϵ_0 is the electrical permittivity of vacuum (8.854×10^{-12} F/m), Z_i and Z_j are atomic numbers of the two atoms (i.e., Ar: 18, P: 15), e is the electron charge (-1.602×10^{-19} C), $a = 0.123$ (for Ar and P) and the function $\phi(x)$ is defined as:

$$\phi(x) = 0.18175e^{-3.19980x} + 0.50986e^{-0.94229x} + 0.28022e^{-0.40290x} + 0.02817e^{-0.20162x}$$

$S(r_{ij})$ is a switching function that ramps the energy function as well as its first/second derivative smoothly to zero between an inner and outer cutoff distance as implemented in LAMMPS. For our CMD simulations, we employ inner and outer cutoff distances of 2.3Å and 3.5Å respectively. The ZBL potential describes the nuclear repulsive interaction between Ar and P atoms at short separation distances in good agreement with DFT calculations (Figure S4). We find that the dispersion corrections (DFT+D3) do not impact the binding energy of Ar-P appreciably

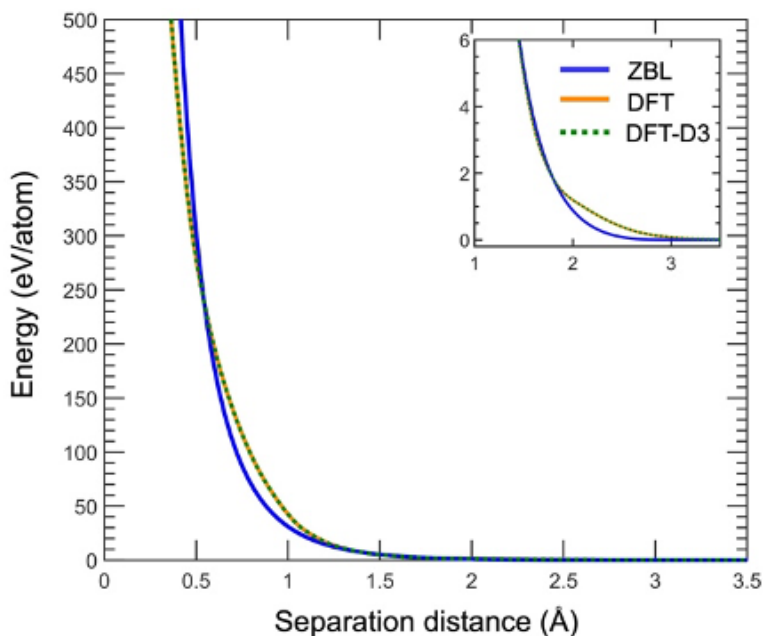


Figure S4. Binding energy of an isolated Ar-P pair held at various separation distances calculated using ZBL, DFT and dispersion-corrected DFT (i.e., DFT+D3). A magnified view of the low energy region is shown in the inset.

3.3 Lennard Jones potential to describe interactions between Argon atoms

We treat the Ar-Ar interactions using a LJ potential, defined as $E = 4\varepsilon [(\sigma/r)^{12} - (\sigma/r)^6]$, where r is the separation distance between the pair of Ar atoms, ε , and σ are independent parameters. This approach is sensible since the interactions between Ar atoms are predominantly dispersive. We take the values of $\varepsilon = 0.0103$ eV and $\sigma = 3.45$ Å for Ar-Ar interactions, which have been successfully used in previous CMD studies of ion-bombardment in two-dimensional MoS₂.⁵⁴ Indeed, the binding energy landscape of an Ar-Ar dimer predicted by LJ is in good agreement with our dispersion-corrected DFT (i.e., DFT+D3) calculations (Figure S5). Furthermore, the binding energy landscape also matches well with a previous parameterization of ReaxFF⁶¹ (Figure S5). Note that these previously published Ar-Ar ReaxFF parameters are not directly transferable to the current study since they do not include low-gradient van der Waals corrections (lg-vdW).⁶¹ The lg-vdW correction term is a key contributor to the accuracy of P-P ReaxFF⁵⁵ in describing the dynamics of formation, migration, and re-organization of structural defects in phosphorene (i.e., the central theme of our study). Thus, we chose to treat the Ar-Ar interactions using a LJ potential instead of ReaxFF.

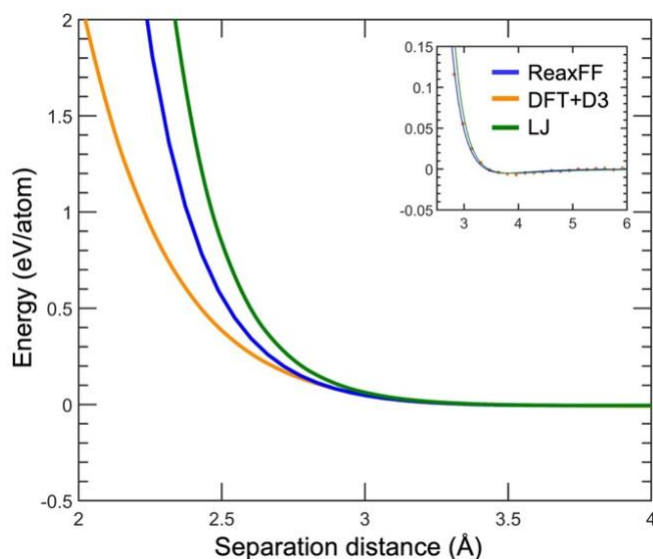


Figure S5. Binding energy of an isolated Ar-Ar pair held at various separation distances calculated using LJ, ReaxFF (parameters from Ref. 61) and dispersion-corrected DFT (i.e., DFT+D3). A magnified view of the depth of the potential well is shown in the inset. For clarity, the DFT + D3 values are shown by open circles in the inset.

4. *Ab initio* molecular dynamics simulations of healing of a small representative hole in ML-phosphorene

To validate the defect healing mechanisms predicted by ReaxFF, we performed *ab initio* molecular dynamics (AIMD) simulations within the framework of dispersion-corrected DFT to investigate the healing of a small representative hole with 3 missing P atoms at 700 K. AIMD simulations are performed using plane-wave formalism within generalized gradient approximation (GGA) as implemented in the VASP package.^{7, 8} Dispersion corrections are accounted using the Grimme D3 scheme.¹⁰ To describe the exchange correlation, we employ the Perdew-Burke-Ernzerhof (PBE) functional with the PAW pseudopotentials (P: $3s^2 3p^3$) supplied by VASP.⁹ The plane wave energy cut off is set at 500 eV, while the Brillouin zone is sampled at Γ point only. We employed a computational supercell of ML-phosphorene, with dimensions $1.98 \text{ nm} \times 1.82 \text{ nm} \times 1.1 \text{ nm}$ (96 P atoms). Periodic boundary conditions are employed along all the directions. Next, we create a small representative hole with 3 missing P atoms as shown in Figure S7(a). We monitor the structural evolution of defective phosphorene within a AIMD run at 700 K for 30 ps (Figure S6, and Supplementary Movie S2).

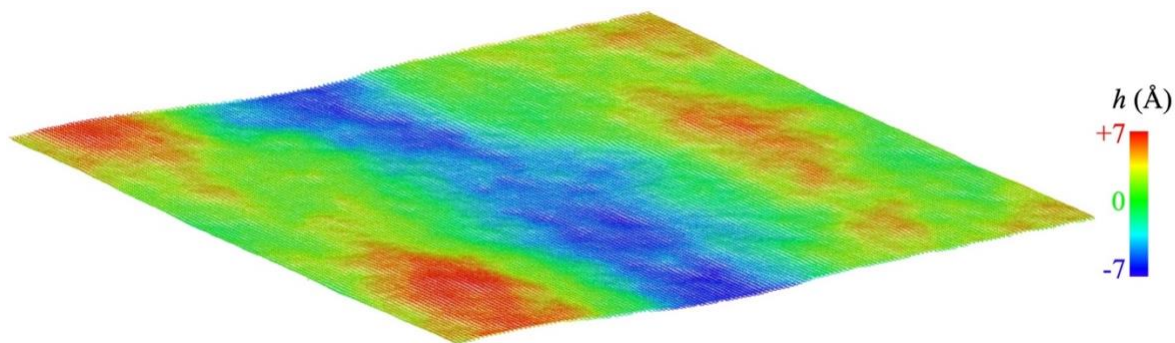


Figure S6. Atomic snapshot of the phosphorene sheet at equilibrium under ambient conditions as obtained from our NPT-MD simulations. The atoms are colored by their height h relative to the mean position of the sheet.

Initially, ML-phosphorene features a small hole ($\sim 6.7 \text{ \AA} \times 4.5 \text{ \AA}$; tri-vacancy) in which three P-P bonds are missing from the atomic network (Figure S7(a)). Two pairs of closely separated atoms along the edge of this hole, namely 1-2 and 3-4 are $\sim 3.31 \text{ \AA}$ and 3.52 \AA apart. During annealing at 700 K, the thermal fluctuations yield substantial rippling of the sheet, which facilitates a wide range of atomic motions, including bond rotation, angle bending and dihedral twisting. In particular, the angle between 9-1-2 triplet changes significantly by $\sim 18^\circ$ within the first 0.87 ps ($t = 0$: 108.7° ; $t = 0.87 \text{ ps}$: 126.5° ; Figures S7 (a,b)). Such angle bending results in the formation of a new bond between atoms 1 and 2 (at $t = 0.87 \text{ ps}$, 1-2 distance is 2.25 \AA), and local healing of the sheet with a 5-membered ring (Figure S7(b)). Similarly, a new bond forms between atoms 3 and 4 (distance at $t = 0.87 \text{ ps}$: 2.29 \AA) to heal the network with a new 5-membered ring. Thereafter, significant twisting of two dihedrals 1-9-11-12, and 1-9-11-13 occur, which causes (a) cleavage of 9-10 bond, (b) formation of new bonds 10-11 and 11-13, and (c) local healing of the hole via formation of one 5-, two 7-, and one 8-membered rings within the next $\sim 5.5 \text{ ps}$ (Figure S7(c)). A series of similar well-coordinated bond rotation, angle bending, dihedral twisting, and ring rearrangement motions eventually result in formation of a coherent atomic network with 5-8 membered rings.

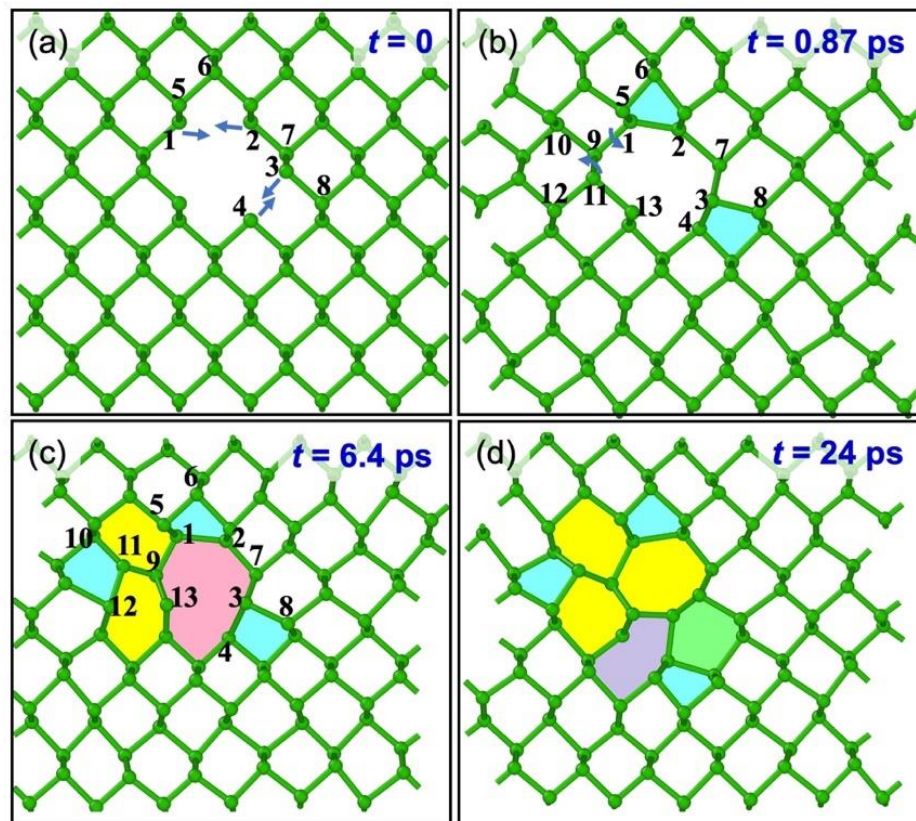


Figure S7. Dynamic processes underlying healing of a representative hole in ML phosphorene as illustrated by AIMD simulations at 700 K. (a) Atomic snapshot of a representative small hole comprising 3 missing P atoms. This hole heals during via intermediate steps (b-c) that feature re-arrangement of rings, bond rotation, and formation of new P-P bonds involving atoms labeled 1-13. Such coordinated atomic motions eventually result in (d) a coherent network composed of 5-8 membered rings. In panels (c) and (d), the newly formed rings are colored by their size, with 5-, 6-, 7-, 8- and 9- membered rings depicted by cyan, green, yellow, purple and pink colors respectively

5. Captions for Supplementary Movies

Supplementary Movie 1: CMD movie showing the atomic-scale mechanisms underlying complete healing of a representative small void ($\sim 1.6 \text{ nm} \times \sim 0.4 \text{ nm}$) formed in phosphorene irradiated at low Ar dose ($2.86 \times 10^{13} \text{ Ar/cm}^2$). CMD trajectory highlights the collective effect of a series of cooperative atomic motions including thermal rippling, formation of new P-P bonds, bond rotation, angle bending and dihedral rotation that eventually repair the void to yield a cohesive lattice with defects. This ring re-arrangement mechanism dominates the relaxation dynamics of phosphorene sheets irradiated at low Ar doses.

Supplementary Movie 2: AIMD movie showing the atomic-scale mechanisms underlying complete healing of a small representative hole with three missing phosphorus atoms. AIMD trajectory shows a healing mechanism similar to that predicted by ReaxFF, which instills confidence in the long-time defect dynamics described by ReaxFF.

Supplementary Movie 3: CMD movie showing the atomic-scale mechanisms underlying coalescence of two closely located large nanopores formed in phosphorene irradiated at high Ar dose ($> 1.43 \times 10^{14}$ Ar/cm²). CMD trajectory elucidates that formation of new P-centered tetrahedra around the edges of the nanopores and their 3D networks underlies coalescence of the nanopores. This mechanism dominates the relaxation dynamics of phosphorene sheets irradiated at high Ar doses.

References

1. Lehtinen, O.; Kotakoski, J.; Krasheninnikov, A. V.; Tolvanen, A.; Nordlund, K.; Keinonen, J., Effects of ion bombardment on a two-dimensional target: Atomistic simulations of graphene irradiation. *Physical Review B* **2010**, *81* (15), 153401.
2. Lehtinen, O.; Dumur, E.; Kotakoski, J.; Krasheninnikov, A. V.; Nordlund, K.; Keinonen, J., Production of defects in hexagonal boron nitride monolayer under ion irradiation. *Nuclear Instruments and Methods in Physics Research Section B: Beam Interactions with Materials and Atoms* **2011**, *269* (11), 1327-1331.
3. Ghorbani-Asl, M.; Kretschmer, S.; Spearot, D. E.; Krasheninnikov, A. V., Two-dimensional MoS₂ under ion irradiation: from controlled defect production to electronic structure engineering. *2D Materials* **2017**, *4* (2), 025078.
4. Vierimaa, V.; Krasheninnikov, A. V.; Komsa, H.-P., Phosphorene under electron beam: from monolayer to one-dimensional chains. *Nanoscale* **2016**, *8* (15), 7949-7957.
5. Lehtinen, O.; Kotakoski, J.; Krasheninnikov, A. V.; Tolvanen, A.; Nordlund, K.; Keinonen, J., Effects of ion bombardment on a two-dimensional target: Atomistic simulations of graphene irradiation. *Physical Review B* **2010**, *81* (15).
6. Taioli, S., Enabling Materials By Dimensionality: From 0D to 3D Carbon-Based Nanostructures. In *Theoretical Chemistry for Advanced Nanomaterials: Functional Analysis by Computation and Experiment*, Onishi, T., Ed. Springer Singapore: Singapore, 2020; pp 135-200.
7. Kresse, G.; Furthmuller, J., Efficiency of ab-initio total energy calculations for metals and semiconductors using a plane-wave basis set. *Computational Materials Science* **1996**, *6* (1), 15-50.
8. Kresse, G.; Furthmuller, J., Efficient iterative schemes for ab initio total-energy calculations using a plane-wave basis set. *Physical Review B* **1996**, *54* (16), 11169-11186.
9. Perdew, J. P.; Burke, K.; Ernzerhof, M., Generalized gradient approximation made simple. *Physical Review Letters* **1996**, *77* (18), 3865-3868.
10. Grimme, S.; Ehrlich, S.; Goerigk, L., Effect of the damping function in dispersion corrected density functional theory. *Journal of Computational Chemistry* **2011**, *32* (7), 1456-1465.
11. Ziegler, J. F.; Biersack, J. P., The stopping and range of ions in matter. In *Treatise on heavy-ion science*, Springer: 1985; pp 93-129.
12. Plimpton, S., Fast Parallel Algorithms for Short-Range Molecular Dynamics. *J. Comput. Phys.* **1995**, *117* (1), 1-19.